https://doi.org/10.5194/essd-2021-429
Preprint. Discussion started: 13 December 2021

Open Access Earth System Science Data Discussions

Permafrost, active layer and meteorological data (2010–2020) from a relict permafrost site at Mahan Mountain, Northeast of Qinghai-Tibet Plateau

Tonghua Wu[1,2*], Changwei Xie[1], Xiaofan Zhu[1], Jie Chen[1], Wu Wang[1], Ren Li[1], Amin Wen[1], Peiqing Lou[1], Dong Wang[1], Chengpeng Shang[1], Yune La[1], Xianhua Wei[1], Xin Ma[1], Yongping Qiao[1], Xiaodong Wu[1], Qiangqiang Pang[1], Guojie Hu[1]

[1] Cryosphere Research Station on the Qinghai-Tibet Plateau, State Key Laboratory of Cryospheric Science, Northwest Institute of Eco-Environment and Resource, Chinese Academy of Sciences, Lanzhou, Gansu 730000, China

[2] Southern Marine Science and Engineering Guangdong Laboratory (Guangzhou), 511458, China

*Correspondence: Tonghua Wu (thuawu@lzb.ac.cn)

https://doi.org/10.5194/essd-2021-429
Preprint. Discussion started: 13 December 2021

Open Access Earth System Science Data Discussions

Abstract: Relict permafrost presents an ideal opportunity to understand the impacts of climatic warming on the ground thermal regime since it is characterized by mean annual ground temperature close to 0 ºC and relatively thin permafrost. The long-term and continuous observations of permafrost thermal state and climate background are of great importance to reveal the links between the energy balance on hourly to annual timescales, to evaluate the variations of permafrost thermal state over multi-annual periods and to validate the remote sensing dataset. Until now there are few data available in relict permafrost regions although those data are important to understand the impacts of climate changes on permafrost especially in the boundary regions between permafrost and seasonally frozen ground regions. In this study, we present 11 years of meteorological and soil data in a relict permafrost site of the Mahan Mountain on the northeast of the Qinghai-Tibet Plateau. The meteorological data are comprised of air and ground surface temperature, relative humidity, wind speed and direction, shortwave and longwave downward and upward radiation, water vapor pressure, and precipitation on half-an-hour timescale. The active layer data include daily soil temperature and soil moisture at five different depths. The permafrost data consist of ground temperature at twenty different depths up to 28.4m. The high-quality and long-term datasets are expected to serve as accurate forcing data in land surface models and evaluate remote-sensing products for a broader geoscientific community. The datasets are available from the National Tibetan Plateau/Third Pole Environment Data Center (https://doi.org/10.11888/Cryos.tpdc.271838, Wu and Xie, 2021).

1 Introduction

Permafrost is defined as ground that remains at or below 0 ºC for at least two consecutive years (Van Everdingen, 1998). As a major component of the cryosphere, permafrost covers about 24 % of the terrestrial landscape (15 million km^2) in the Northern Hemisphere (Brown et al., 1998; Zhang et al., 2000; Boike et al., 2019; Obu et al., 2019). The active layer, which is the top layer of ground subject to annual thawing and freezing in areas underlain by permafrost, plays an important role in cold regions because most ecological, hydrological, biogeochemical, and pedogenic activities take

https://doi.org/10.5194/essd-2021-429
Preprint. Discussion started: 13 December 2021

place within it (Hinzman et al., 1991; Kane et al., 1991; Nelson et al., 2000). The thermal state of permafrost is sensitive to climatic warming. There are more and more evidences indicate that permafrost is warming at both global and regional scales (Harris et al., 2003; Cheng and Wu, 2007; Romanovsky et al., 2010; Zhao et al., 2010; Hjort et al., 2018; Biskaborn et al., 2019). Generally, the evidence of permafrost degradation includes rising mean annual ground temperature, deepening active layer thickness, talik and thermokarst development, and decreasing permafrost extent (Cheng and Wu, 2007). Permafrost degradation would affect local hydrology, ecosystem, infrastructure stability, and even feedback to the climate system (Nauta et al., 2015; Walvoord and Kurylyk, 2016; Hjort et al., 2018).

The relict permafrost is usually characterized with high-temperature sporadic permafrost, where the mean annual ground temperature of permafrost is close to 0 ºC. The relict permafrost presents a favorable opportunity to compare the impacts of climatic warming on the permafrost and the seasonal frozen ground, as they have similar climate conditions (Mu et al., 2017). In addition, the different impacts of vegetation, terrain and organic matters in ground surface on the ground thermal regime could be figured out in the relict permafrost regions (Xie et al., 2013). The long-term and continuous observations of meteorological variables, active layer, and permafrost are of great importance to understand the impacts of climatic changes on ground thermal regime. It is critical to better understand the energy balance at the ground surface in order to enhance our understanding of the heat and moisture exchanges within the active layer and the permafrost layer. Furthermore, the data on atmospheric conditions and hydrothermal regime of the active layer are also of great significance for validating remote sensing dataset and land surface models in cold regions (Westermann et al., 2011; Park et al., 2016; Park et al., 2018; Che et al., 2019; Zhao et al., 2021). However, there are few data available for the relict permafrost regions, especially on the active layer and permafrost temperature data. As for the Qinghai-Tibet Plateau, the high-quality and long-term datasets of meteorological and permafrost data are relatively scarce especially in the relict permafrost regions on account of limited logistic support, expensive maintenance cost, and difficult living environments (Li et al., 2020). It is of great importance to share the good data for addressing the challenges of climate change and its impacts on permafrost (Li et al., 2021). In this paper, the presented data include hourly meteorological variables, daily soil temperature and soil moisture, monthly permafrost temperature, and soil physical parameters from a relict permafrost site at the Mahan Mountain on the northeast of the Qinghai-Tibet Plateau.

The Mahan Mountain relict permafrost observation site on the northeast of the Qinghai-Tibet Plateau had been established by the Cryosphere Research Station on the Qinghai-Tibet Plateau, the Northwest Institute of Eco-Environment and Resource, the Chinese Academy of Sciences since 2009. Before the establishment of this observation site, a small permafrost region was found in the fracture bedrock on the Mahan Mountain (Li et al., 1986). Researchers found that the permafrost on the Mahan Mountain is vulnerable to the climate warming based on borehole measurements (Li et al., 1993). The characteristics and persistence of relict high-altitude permafrost on the Mahan Mountain has been demonstrated by Xie et al. (2013).

We present standard meteorological data, including air and ground surface temperature, relative humidity, water vapor pressure, wind speed and direction, shortwave downward and upward radiation, longwave downward and upward radiation, and precipitation. The data cover an 11-year span from January 1 2010 to December 31 2020. In addition, field measurement for soil physical parameter at different depths of five sampling sites from October 2015 to August 2016 are also presented, including soil bulk density, soil gravimetric water content, and soil porosity.

2 Data description

2.1 Site description

The Mahan Mountain permafrost site (35°44′N and 103°58′E, 3670 m a.s.l.) is located on the northeast Qinghai-Tibet Plateau, which is the peak of the Chinese Loess Plateau (Fig. 1) (Xie et al., 2013). Relict permafrost was discovered by Li (1986) in fractured bedrock on the Mahan Mountain and was considered as “living fossil” of permafrost on the Chinese Loess Plateau. From 1991 to 1993, Li et al. (1993) had drilled 12 boreholes across four transects to evaluate the occurrence of permafrost.

https://doi.org/10.5194/essd-2021-429
Preprint. Discussion started: 13 December 2021

Among them, 6 boreholes had shown obvious evidences indicating permafrost occurrence. The permafrost mostly emerged in the moist depression regions where vegetation is well developed. The original permafrost area was approximately 0.16 km^2, while the area of which reduced to 0.13 km^2 recently. The mean annual ground temperature ranges from -0.2 to -0.3℃, which belongs to typical warm permafrost (Cheng and Wu, 2007). The permafrost thickness is about 5 - 40m, and the active layer thickness ranges from 1.0 to 1.5m (Li et al., 1993; Dong et al., 2013; Liu et al., 2015). The existence of abundant peat layer and ground ice can exert effective protective effect to the underlying permafrost. Thus, despite permafrost extent is very small, the permafrost would be not disappearing in the next 40 to 50 years by model prediction under current warming trends (Xie et al., 2013).

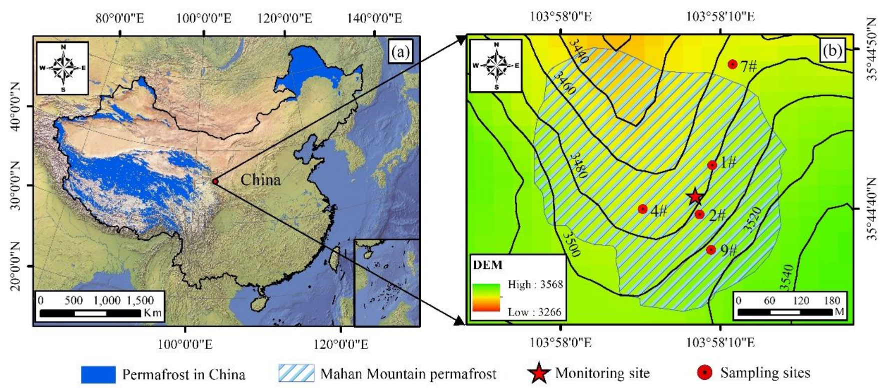

Figure 1. Location (a), topographical map and observation site (b) of the Mahan Mountain relict permafrost region. Permafrost distribution data in China is derived from Zou et al. (2017) and Zhang et al. (2019), and the Environmental and Ecological Science Data Center for West China (http://westdc.westgis.ac.cn). The permafrost distribution of the Mahan Mountain is derived based on field survey.

The climate condition on the Mahan Mountain is cold and sub-humid. Observed mean annual air temperature on the relict permafrost region is about -1.4℃ from 2010 to 2020, and the duration of negative air temperature exceeds 200 days. Local ground surface is covered by the swamp meadow with around 90% coverage. The dominant plant types mainly include *Kobresia humilis*, *K. pygmaea* and *K. capilifolia* (Sun and

Zhao, 1995). Abundant hummocks are well-developed, which are influenced by high moisture content and frost heaving effect. Greater ecosystem respiration rate and soil carbon release occurred in the relict permafrost region in comparison with the Arctic permafrost region (Mu et al., 2017).

2.2 Data description

The Mahan Mountain meteorological and permafrost observation site were set up in 2009. The observation details was shown in Fig. 2 and Table 1. There is a regularly manual manintenance every one or two months, mainly including power system checking, sensor and field cleaning, and data collecting; In addition, due to the independent power energy from three solar panels, the meteorological data were continuous with high data quality.

For the active layer soil temperature and moisture observations, there existed several blank gaps from from 2012 to 2014 owing storage battery broken. Subesequently, we solve these problems by installing new storage battery with larger capacity. Moreover, the permafost borehole suffered water penetration from 2012 to 2016, which caused low quality permafrost temperature data, and we repaired it and manually measured the permafrost temperature at different depths since 2017. Related data introdution was as follows.

https://doi.org/10.5194/essd-2021-429
Preprint. Discussion started: 13 December 2021

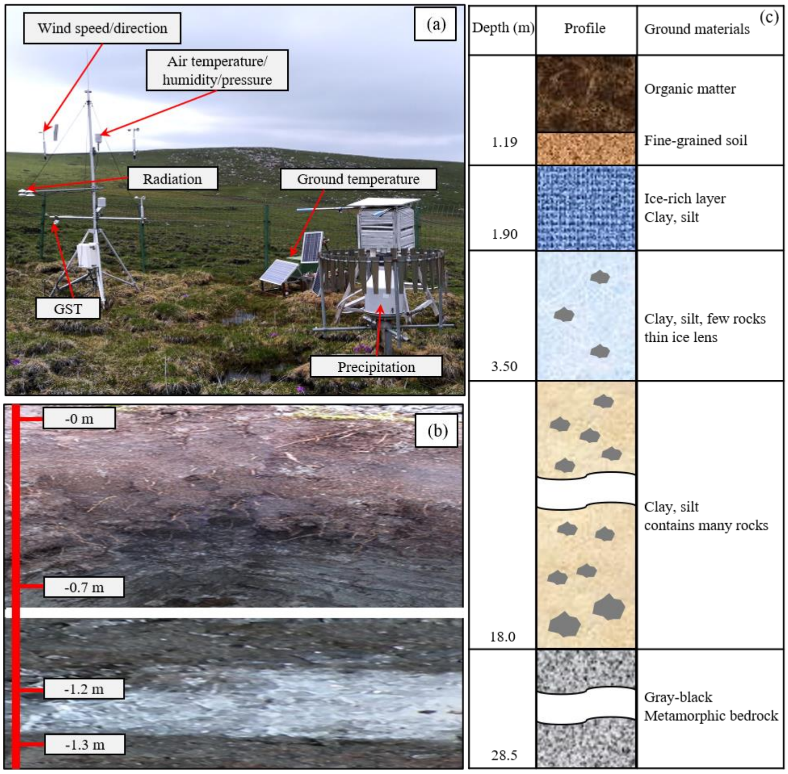

Figure 2. The setup of the meteorological and permafrost observation site in the Mahan Mountain. The meteorological monitoring parameters mainly includes: wind speed and direction, air humidity, radiation, ground surface temperature (GST) and precipitation (a); active layer soil profile and ground ice near permafrost table (b); soil profiles information of the permafrost borehole (c).

2.2.1 Meteorological condition

The meteorological station of the Mahan Mountain continues to observe a variety of meteorological variables from January 1, 2010 to December 31, 2020 (Table 1). All meteorological variables are monitored in 30-minutes interval (Fig. 2), and the monitoring data are recorded by a CR1000 data logger (Campbell Scientific, Inc.). Because the weather observation equipment is regularly maintained, most of the meteorological data have high quality and continuity with very limited missing data. The detailed description of each meteorological variable is as follows.

Table 1. List of sensors, accuracy, measuring height and interval, and operation period for

https://doi.org/10.5194/essd-2021-429
Preprint. Discussion started: 13 December 2021

156 meteorological variables at the Mahan Mountain.

Variable	Sensor	Range	Accuracy	Sensor height	Measuring interval	Operation period	Unit
Shortwave radiation	CM3, Kipp & Zonen, Netherlands	0 to 2000 W/m^2	<5%	2m	30min	Jan 2010 – Dec 2020	W/m^2
Longwave radiation	CM3, Kipp & Zonen, Netherlands	0 to 2000 W/m^2	<10%	2m	30min	Jan 2010 – Dec 2020	W/m^2
Air temperature	HMP45C,Vaisala Finland	-40 to 60 °C	±0.2-0.5°C	2m, 4m	30min	Jan 2010 – Dec 2020	°C
Relative humidity	HMP45C,Vaisala Finland	0 to 100 % RH	±3%	2m, 4m	30min	Jan 2010 – Dec 2020	%
Wind speed/direction	014A, MetOne, USA	0 to 45 m/s	0.11m/s	2m	30min	Jan 2010 – Dec 2020	m·s^{-1}/ Deg
Water vapor pressure	HMP45C,Vaisala Finland	-	±3%	2m, 4m	30min	Jan 2010 – Dec 2020	hPa
Precipitation	T200B3 precipitation gauge	0 to 1000 mm	0.1%	1.6m	30min	Jan 2010 – Dec 2020	mm
Ground surface temperature	IRR-P,Vaisala Finland	-55 to +80 °C	± 0.3℃	2m	30min	Jan 2010 – Dec 2020	°C

https://doi.org/10.5194/essd-2021-429
Preprint. Discussion started: 13 December 2021

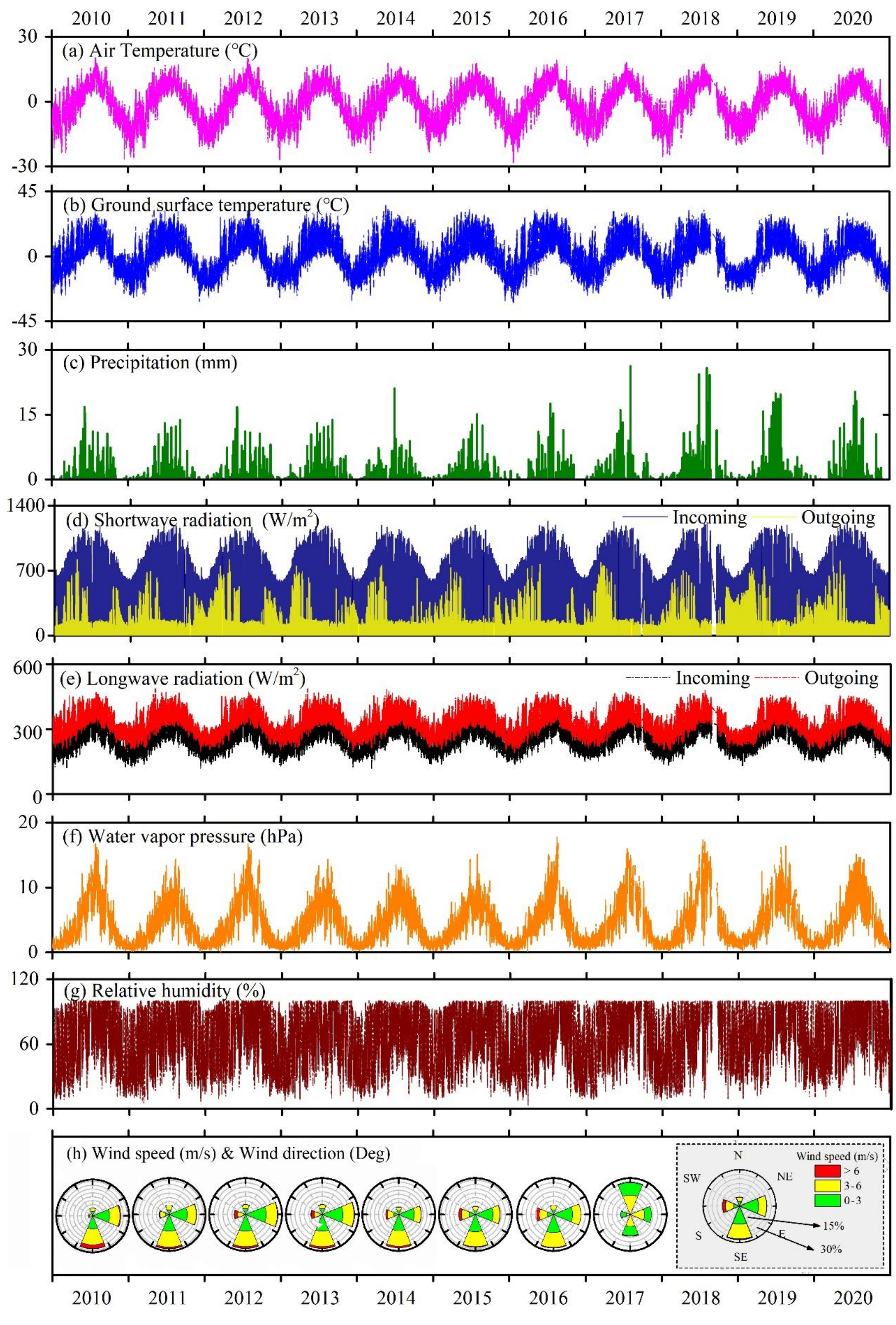

Figure 3. Time series of meteorological variables from 2010 to 2020 at the Mahan Mountain, including air temperature (a), ground surface temperature (b), precipitation (c), shortwave radiation (d), longwave radiation (e), water vapor pressure (f), relative humidity (g), wind speed & direction

https://doi.org/10.5194/essd-2021-429
Preprint. Discussion started: 13 December 2021

(h).

Air and ground surface temperature

Air temperature was measured by shielded HMP45C at heights of 2m and 4m above the ground surface. Such sensors were relatively stable and the data integrity reached to almost 100% with an accuracy of 0.2-0.5℃. During 2010-2020, the mean annual air temperature was ranging from -2.0°C to -0.7°C (Fig. 3a).

The ground surface temperature (GST) was measured by the IRR-P at a height of 2 m above the ground surface through non-contact infrared radiation. In the Mahan Mountain permafrost site, the GST was ranging from -33.2°C to 36.9°C. The lowest mean annual GST was -2.1°C occurred in 2012, while the highest one was -0.6°C in 2016, and the 11-years mean GST was -1.4°C (Fig. 3b).

Precipitation

A Geonor T-200B precipitation gauge (1000 mm capacity) was installed at the height of 1.6m above ground surface. There is a vibrating-wire sensor within the gauge to measure the total weight of a collection bucket, and a single Alter shield around the gauge can guarantee higher catch ratio to some extent. In general, the accuracy and sensitivity of this gauge is 0.1% and 0.1mm, respectively. This gauge has been widely used to as the reference standard in the WMO Solid Precipitation Intercomparison Experiment (WMO-SPICE) (Nitu et al., 2018) and related precipitation intercomparison experiments (Zhao et al., 2021). Due to the influence of wind disturbance, wetting loss and evaporation loss, there exists some abnormal precipitation values. To guarantee the data quality, we have checked related records to decide whether a precipitation event occurring or not by combining with synchronous air temperature and ground surface temperature, shortwave radiation, and relative humidity data, and related data are also corrected according to the reference of Domine et al. (2021).

Observed local mean annual precipitation was 318.6 ± 54.3 mm from 2010 to 2020, the minimum and maximum annual precipitation occurred in 2015 and 2018 with 258.3mm and 443.9mm, respectively, which also showed an increasing trend during

https://doi.org/10.5194/essd-2021-429
Preprint. Discussion started: 13 December 2021

this period (Fig. 3c). In addition, approximate 80% annual precipitation concentrate in the period of May to September, but only no more than 5% precipitation occurs in winter.

Radiation

Upward/downward shortwave and longwave radiations were measured by the Kipp & Zonen CM3 radiometer. The spectrum range of the shortwave and longwave radiometers are from 0.3 μm to 2.8 μm and from 4.5 μm to 42 μm, respectively. In the Mahan Mountain, the downward shortwave radiation tended to reach its maximum in spring, followed by summer, and lowest in winter and autumn. Upward shortwave radiation also reached its maximum in spring, but the difference was that the downward shortwave radiation in summer is comparable to that of autumn and winter, or even lower, which mainly due to the cloudy and rainy weather in summer. The maximum values of upward/downward longwave radiation usually occurred in summer, followed by autumn, while the values in winter and spring tended to be lower, which shows similar patterns with the seasonal variations of ground surface temperature and air temperature.

Relative humidity and water vapor pressure

The relative humidity was measured by shielded HMP45C probes at heights of 2m and 4m above the ground surface. However, when in heavy rainfall or fog weather, the observed relative humidity might exceed its physical limits, i.e., 0-100%. In this case, the relative humidity was corrected to 100% instead (Fig. 3g). The variations of relative humidity were consistent with rainfall events and the variations of air temperature.

The water vapor pressure was calculated from the relative humidity at heights of 2m and 4m above the ground surface. Water vapor pressure generally reached its maximum in summer, followed by autumn, and lowest in spring and winter, which showed obvious seasonal variations (Fig. 3f).

Wind speed and wind direction

https://doi.org/10.5194/essd-2021-429
Preprint. Discussion started: 13 December 2021

The 014A MetOne wind speed and direction sensors were installed at a height of 2m above the ground surface. The negative values for wind directions were replaced by 6999. The wind speed and direction during 2010-2017 were continuous with high quality. Extensive data gaps emerged in the wind direction due to equipment problems after August 27, 2017. The wind speed data gradually became unavailable after 2019. The wind speed mainly stayed between 2 and 6 m/s (Fig. 3h).

2.2.2 Active layer hydrothermal condition

Soil temperature and soil moisture

The underground soil temperature (ST) and volumetric water content (VWC) data in the active layer were monitored at five depths (-10cm, -30cm, -80cm, -100cm, -120cm). The ST data were measured by 105T/109 thermistors (Campbell Scientific, USA) with an accuracy of ± 0.1°C. The VWC data were measured by the time-domain reflectometry (TDR-100, Campbell Scientific, USA) with an accuracy of ±3%. These sensors were all attached to a CR1000 data logger (Campbell Scientific, USA) at 30 minutes intervals. We finally resampled the ST and VWC data into daily data.

Table 2. List of sensors, accuracy, measuring height and interval, and operation period for soil temperature and soil moisture within the active layer at the Mahan Mountain satiation.

Variable	Sensor	Range	Accuracy	Depth/cm	Measuring interval	Operation period	Unit
Soil temperature	105T, Campbell	-78 to +50 °C	±0.1°C	-10, -30, -80, -100, -120	30min	Jan 2010 – Dec 2020	°C
Soil moisture	TDR-100, Campbell	0 to 100%	±3%	-10, -30, -80, -100, -120	30min	Jan 2010 – Dec 2020	m^3m^{-3}

To obtain high accurate data, the quality control was made by manually checking whether there were abnormal or missing data. For the ST data, the missing ST data accounted for 17.1% during the period of 2010-2020. The major ST data gaps were from 23 November 2013 to 21 September 2014. Besides, we checked the ST data based on the zero-curtain effect, assuming that the soil properties and water composition does not change during 2010-2020. For the VWC data, the missing and abnormal data were approximately occupying 30.7% of the entire VWC data mainly from 2012 to 2014. If the VWC data was only missed in several hours within a day, we interpolated the missing data with proximity averaging method. In the case of missing data persist for a longer time, we filled them with 6999. Overall, all the missing or abnormal ST and VWC data were replaced as 6999.

According to the ST profile (Fig. 4), the ST in the active layer shows a seasonal dynamic change. The thawing onset was generally in the middle of April, and the maximum thawing depth was reached in late September. The amplitude of ground temperature in the active layer decreased rapidly with increasing soil depths. The minimum and maximum values of ST data at depths of 10cm, 30cm, 80cm ,100cm and 120cm were -8°C and 9.8°C, -6.4°C and 8.4°C, -3.1°C and 3.5°C, -1.4°C and 1.9°C, -0.74°C and 0.7°C, respectively. The mean annual ST in 2019 reached its maximum during 2010-2020.

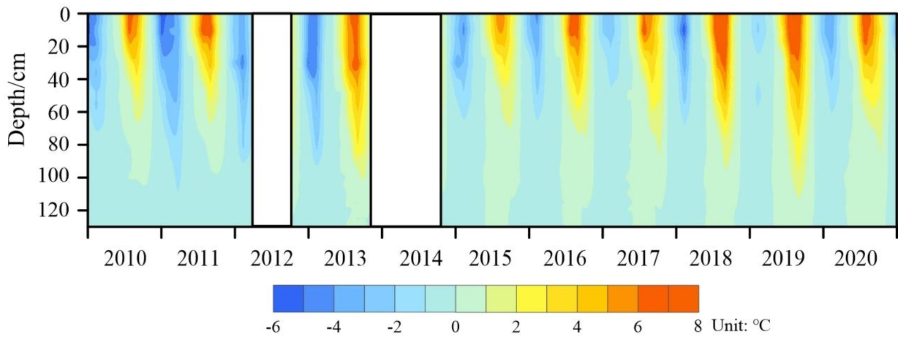

Figure 4. Active layer soil temperature profiles during 2010-2020 at the Mahan Mountain permafrost site. The blank gap stands for the major missing data from 21 March 2012 to 9 September 2012, and from 23 November 2013 to 21 September 2014, respectively.

As shown in Fig. 5, there were two higher VWC zones in the upper and lower part of active layer, which were located at around 0–40cm and 90–110cm depths, respectively, and a relatively lower VWC was in the middle part of active layer. In the thawing season, the VWC reached to around 0.7 m^3 m^{-3} in upper and lower part of active layer, and was approximately 0.3 to 0.4 m^3 m^{-3} in the middle part of active layer. In the freezing season, there were significant differences to thawing season, the VWC

https://doi.org/10.5194/essd-2021-429
Preprint. Discussion started: 13 December 2021

in middle part of active layer was higher than that of the upper and lower part of active layer. Moreover, the VWC at 40–90cm depths exhibited a rapid increase in the freezing season since 2015, which could reach to 0.4 m^3 m^{-3}, and the VWC at around 120cm depth showed a rapid increase in freezing season since 2017, with a slightly lower VWC than that of the 40-90cm depths.

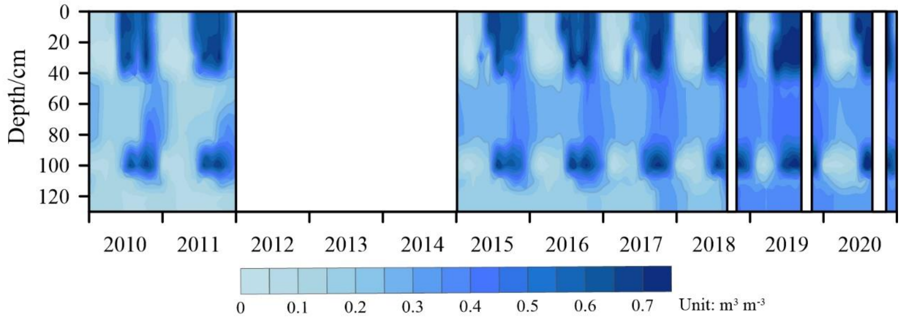

Figure 5. Evolution of the soil moisture profiles from 2010 to 2020 at the Mahan Mountain permafrost site. The blank gap stands for the missing data from 1 January 2012 to 6 January 2015, from 27 August 2018 to 21 September 2018, from 12 September 2019 to 24 October 2019, and from 25 September 2020 to 6 November 2020.

Soil physical parameter

From October 2015 to August 2016, field measurement for soil physical parameter data was carried out by test pit probing and sampling soils, including soil gravimetric water content, soil bulk density, and soil porosity. There are five sampling sites in total. Four sites (1#, 2#, 4# and 9#) located in the permafrost region, where the vegetation type is dominated by swamp meadow. Site 7# located in seasonally frozen ground region, where the vegetation type is mainly alpine meadow (Table 3). These data can be used to as the input parameters in relevant permafrost and land surface process model.

Table 3 Information of field sampling site for soil physical parameters from October 2015 to August 2016 at the Mahan Mountain.

Sampling site	Elevation (m)	Vegetation type	Frozen soil type
1#	3576.4	Swamp meadow	Permafrost
2#	3576.9	Swamp meadow	Permafrost

4#	3577.2	Swamp meadow	Permafrost
7#	3567.0	Alpine meadow	Seasonally frozen ground
9#	3578.7	Swamp meadow	Permafrost

Soil samples were obtained in each soil layer using a standard soil sampler (5 cm diameter and 5–cm–high stainless-steel cutting ring). The soil bulk density is estimated using the oven-dry method. Soil porosity is the ratio of nonsolid volume to the total volume of soil, which is calculated by soil bulk density and specific weight of soil (Zhao and Sheng, 2015; Indoria et al., 2020). As shown in Table 4, the soil bulk density and soil porosity in 4#, 7# and 9# sites present significant differences at different depths. 7# site that located in the seasonally frozen ground shows larger soil bulk density ranging from 0.66 to 1.27 g/cm^3. As soil depth increases, the soil bulk density of 4# and 7# sites become larger. Soil porosity also show obvious differences among the three sites, whereas the shallow soil layers exhibit greater porosity than deep soil layers. Soil porosity of 4# site ranges from 69.7% to 85.5%, where the maximum values are found at depths of 0-40cm.

Table 4 Soil bulk density and soil porosity within the active layer at different depths from Oct 2015 to Aug 2016 at the Mahan Mountain. The location and information of sampling sites can be seen in Figure 1(b) and Table 3, respectively.

Depth (cm)	Soil bulk density (g/cm^3)			Soil porosity (%)		
	4#	7#	9#	4#	7#	9#
0-10	0.34	0.66	0.45	85.5	74.3	81.0
10-20	0.56	0.92	0.53	76.0	65.4	76.9
20-30	0.41	0.84	0.55	81.1	68.4	75.6
30-40	0.37	1.03	0.56	84.5	61.8	74.5
40-50	0.67	1.27	0.43	74.7	53.4	76.3
50-60	0.82	null	0.46	69.7	null	83.9
60-70	0.62	null	0.45	77.1	null	83.1

Note: “null” stands for no samples.

Moreover, gravimetric soil water content (GWC) was measured by using oven

https://doi.org/10.5194/essd-2021-429
Preprint. Discussion started: 13 December 2021

drying method (Zhao and Sheng, 2015). The GWC is the ratio between the absolute weights of wet and dry soil samples, which can be measured after drying 24h at 105℃. The GWC at five sites show similar profile features. Overall, the GWC gradually decrease with increasing soil depths (Fig. 6). The GWC in the four permafrost sites (1#, 2#, 4#, and 9#) shows similar patterns in depths with their values ranging from 15% to 250%. The GWC in the seasonal frozen ground site (#7) is only 18.5%-77.4%, which is smaller compared to the four permafrost sites (Fig. 6d). In addition, GWC also presents some monthly differences, such as larger values tend to occur in June and July in the layers of 10-40 cm, which may be caused by abundant precipitation and thawing processes during this period.

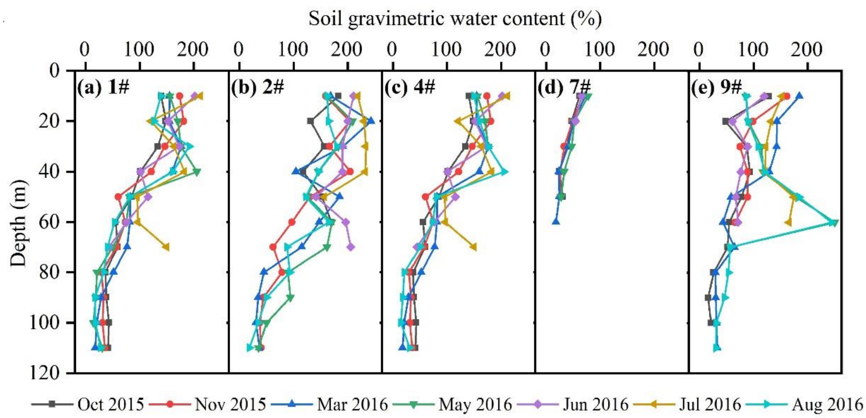

Figure 6. Soil gravimetric water content at five sampling sites (1#, 2#, 4#, 7#, and 9#) from Oct. 2015 to Aug. 2016 at the Mahan Mountain. The location and information of sampling sites can be seen in Figure 1(b) and Table 3, respectively.

2.2.3 Permafrost temperature

In August 2008, a borehole with a depth of 28.5 m was drilled to monitor the permafrost temperature. Twenty thermistors were installed at different depths in the borehole (0.1, 0.4, 0.9, 1.4, 1.9, 2.4, 3.4, 6.4, 7.4, 9.4, 11.4, 13.4, 15.4, 17.4, 19.4, 21.4, 23.4, 25.4, 27.4 and 28.4 m). Thermistor probes made by the Chinese State Key Laboratory of Frozen Soil Engineering at Lanzhou were used to measure the ground temperature. These thermistor probes have a sensitivity of ± 0.05°C in the lab (Cheng

https://doi.org/10.5194/essd-2021-429
Preprint. Discussion started: 13 December 2021

and Wu, 2007). From May 2009, permafrost temperature data for each half-hour was automatically recorded by the datalogger (CR1000, Campbell Scientific, USA). No data was recorded from 2012 to 2016 due to water penetration into borehole. Since 2017, a digital multimeter was used to manually measure the permafrost temperature at 13 layers (3, 4, 5, 7, 9, 11, 13, 15, 17, 19, 21, 23 and 25m) for 2-4 times each month. The quality control is carried out to check whether the data is missing or invalid, which is replaced by 6999 as nodata. The ground temperature is then resampled to monthly data.

The records showed that the permafrost temperature at all depths below 2.0 m was mostly negative all year round. The location of of permafrost base in this site exceeded the drilling depth (28.5 m). The soil temperature in the permafrost layer shows minimum values of around -0.2°C at depths of 10m to 16 m, close to -0.1°C at depths -2.4m to -27.4m, and increased upwards and downwards with a temperature gradient of ± 0.01°C/m (Fig. 7).

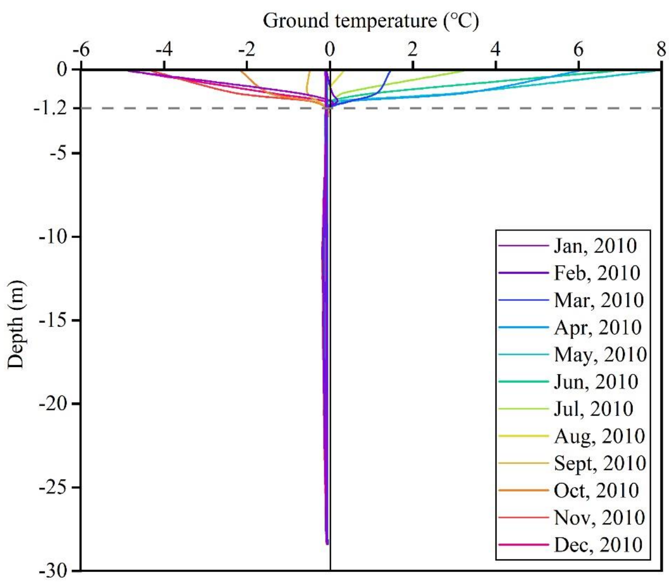

Figure 7. Ground temperature envelopes in the permafrost borehole drilled in 2010 at the Mahan Mountain.

3 Data availability

https://doi.org/10.5194/essd-2021-429
Preprint. Discussion started: 13 December 2021

The dataset has been available and can be freely download from the National Tibetan Plateau/Third Pole Environment Data Center (https://data.tpdc.ac.cn/en/disallow/c0a65170-d7cc-4a10-b3fd-39f813cd1387/, https://doi.org/10.11888/Cryos.tpdc.271838, Wu and Xie, 2021).

4. Conclusions

Mahan Mountain is a relict permafrost site on the northeast of Qinghai-Tibet Plateau where meteorological and active layer hydrothermal data are automatically acquired and the ground temperature data are manually recorded. This site is dedicated to studies of atmosphere-ground surface interactions and permafrost changes. An 11-year time series of meteorological, active layer and permafrost data is provided. These high-quality and long-term observation data have been already used to assess the permafrost model and to project the permafrost changes in the future (Xie et al., 2013). The objective of releasing these data is to improve and validate the permafrost models and land surface models, which confront great difficulties in modelling mountain permafrost dynamics.

Author contributions

Tonghua Wu designed the research and obtained funding. Changwei Xie and Wu Wang deployed and maintained the instruments. Xiaofan Zhu, Jie Chen, Amin Wen, Dong Wang, Peiqing Lou, Chengpeng Shang, Yune La, Xianhua Wei, Xin Ma and Yongping Qiao analyzed the data and prepared the data files. Ren Li, Xiaodong Wu, and Guojie Hu conducted the field work. Tonghua Wu wrote the paper with inputs from the co-authors and coordinated the analysis and contributions from all co-authors.

Competing interests

The authors declare that they have no conflict of interest.

Acknowledgements

This work was financially supported by the CAS "Light of West China" Program, the National Natural Science Foundations of China (41771076, 41690142, 41961144021). We thank in particular Professor Lin Zhao from Nanjing University of

Information Science & Technology for his long-term support to maintain the observation.

References

Biskaborn, B. K., Smith, S. L., Noetzli, J., Matthes, H., Vieira, G., Streletskiy, D. A., Schoeneich, P., Romanovsky, V. E., Lewkowicz, A. G., Abramov, A., Allard, M., Boike, J., Cable, W. L., Christiansen, H. H., Delaloye, R., Diekmann, B., Drozdov, D., Etzelmüller, B., Grosse, G., Guglielmin, M., Ingeman-Nielsen, T., Isaksen, K., Ishikawa, M., Johansson, M., Johannsson, H., Joo, A., Kaverin, D., Kholodov, A., Konstantinov, P., Kröger, T., Lambiel, C., Lanckman, J.-P., Luo, D., Malkova, G., Meiklejohn, I., Moskalenko, N., Oliva, M., Phillips, M., Ramos, M., Britta, A., Sannel, K., Sergeev, D., Seybold, C., Skryabin, P., Vasiliev, A.,Wu, Q., Yoshikawa, K., Zheleznyak,M., and Lantuit, H.: Permafrost is warming at a global scale, Nat. Commun., 10, 264, https://doi.org/10.1038/s41467-018-08240-4, 2019.

Boike, J., Nitzbon, J., Anders, K., Grigoriev, M., Bolshiyanov, D., Langer, M., Lange, S., Bornemann, N., Morgenstern, A., Schreiber, P., Wille, C., Chadburn, S., Gouttevin, I., Burke, E., and Kutzbach, L.: A 16-year record (2002–2017) of permafrost, active-layer, and meteorological conditions at the Samoylov Island Arctic permafrost research site, Lena River delta, northern Siberia: an opportunity to validate remote-sensing data and land surface, snow, and permafrost models, Earth Syst. Sci. Data, 11, 261–299, https://doi.org/10.5194/essd-11-261-2019, 2019.

Brown, J., Ferrians, O. J., Heginbottom, J. A., and Melnikov, E. S.: Circum-Arctic Map of Permafrost and Ground Ice Conditions, Boulder, CO, National Snow and Ice Data Center, digital media, 1998.

Che, T., Li, X., Liu, S., Li, H., Xu, Z., Tan, J., Zhang, Y., Ren, Z., Xiao, L., Deng, J., Jin, R., Ma, M., Wang, J., and Yang, X.: Integrated hydrometeorological, snow and frozen-ground observations in the alpine region of the Heihe River Basin, China, Earth Syst. Sci. Data, 11, 1483–1499, https://doi.org/10.5194/essd-11-1483-2019, 2019.

Cheng, G., and Wu, T.: Responses of permafrost to climate change and their environmental significance, Qinghai-Tibet Plateau, J. Geophys. Res.: Earth Surf., 112, 1-10, https://doi.org/10.1029/2006JF000631, 2007.

Domine, F., Lackner, G., Sarrazin, D., Poirier, M., and Belke-Brea M.: Meteorological, snow and soil data (2013–2019) from a herb tundra permafrost site at Bylot Island, Canadian high Arctic, for driving and testing snow and land surface models. Earth Syst. Sci. Data, 13, 4331-

4348, https://doi.org/10.5194/essd-13-4331-2021, 2021.

Dong, X., Xie, C., Zhao, L., Yao, J., and Hu, G.: Characteristics of surface energy budget components in permafrost region of the Mahan Mountain, Lanzhou (in Chinese). J. Glaciol. Geocryol., 35(2), 320-326, https://doi.org/10.7522/j.issn.1000-0240.2013.0038, 2013.

Harris, C., Mühll, D. V., Isaksen, K., Haeberli, W., Sollid, J. L., King, L., Holmlund, P., Dramis, F., Guglielmin, M., and Palacios, D.: Warming permafrost in European mountains, Glob. Planet. Chang., 39, 215-225, https://doi.org/10.1016/j.gloplacha.2003.04.001, 2003.

Hinzman, L. D., Kane, D. L., and Gieck, R. E: Hydrologic and thermal properties of the active layer in the Alaskan Arctic, Cold Reg. Sci. Technol., 19(2): 95-110, https://doi.org/10.1016/0165-232X(91)90001-W, 1991.

Hjort, J., Karjalainen, O., Aalto, J., Westermann, S., Romanovsky, V. E., Nelson, F. E., Etzelmüller, B., and Luoto, M.: Degrading permafrost puts Arctic infrastructure at risk by mid-century. Nat. Commun., 9, 5147, https://doi.org/10.1038/s41467-018-07557-4, 2018.

Indoria, A. K., Sharma, K. L., Reddy, K. S.: Hydraulic properties of soil under warming climate, in: Climate Change and Soil Interactions, edited by: Edited by: Prasad M. N. V. and Pietrzykowski M., Elsevier, 473-508, https://doi.org/10.1016/B978-0-12-818032-7.00018-7, 2020.

Kane, D. L., Hinzman, L. D., and Zarling J. P: Thermal response of the active layer to climatic warming in a permafrost environment, Cold Reg. Sci. Technol., 19(2): 111-122., https://doi.org/10.1016/0165-232X(91)90002-X, 1991.

Li, S. D.: Permafrost found on Mahan Mountains near Lanzhou (in Chinese). J. Glaciol. Geocryol., 8(4), 409–410, 1986.

Li, X., Che, T., Li, X., Wang, L., Duan, A., Shangguan, D., Pan, X., Fang, M., and Bao, Q.: CASEarth Poles: Big Data for the Three Poles, Bull. Am. Meteorol. Soc., 101(9), E1475–E1491, https://doi.org/10.1175/BAMS-D-19-0280.1, 2020.

Li, X., Cheng, G., Wang, L., Wang, J., Ran, Y., Che, T., Li, G., He, H., Zhang, Q., Jiang, X., Zou, Z., and Zhao, G.: Boosting geoscience data sharing in China, Nat. Geosci., 14, 541–542, https://doi.org/10.1038/s41561-021-00808-y, 2021.

Li, Z., Li, S., and Wang, Yi.: Regional features of permafrost in Mahan Mountain and their relationship to the environment (in Chinese). J. Glaciol. Geocryol., 15(1), 83-89,

https://doi.org/10.5194/essd-2021-429
Preprint. Discussion started: 13 December 2021

https://doi.org/10.12785/amis/070422, 1993.

Liu, W., Xie, C., Zhao, L., Wu, T., Li, R., Wang, W., and Qiao, Y.: Simulating the active layer depth and analyzing its influence factors in permafrost of the Mahan Mountain, Lanzhou (in Chinese). J. Glaciol. Geocryol., 37(6), 1443-1452, https://doi.org/10.7522/j.isnn.1000-0240.2015.0160, 2015.

Mu, C., Wu, X., Zhao, Q., Smoak, J. M.,Yang, Y., Hu, L., and Zhang, T.: Relict mountain permafrost area (LoessPlateau, China) exhibits high ecosystem respiration rates and accelerating rates in response to warming. J. Geophys. Res.: Biogeosci., 122, 2580-2592. https://doi.org/10.1002/2017JG004060, 2017.

Nauta, A. L., Heijmans, M. M. P. D., Blok, D., Limpens, J., Elberling, B., Gallagher, A., Li, B., Petrov, R.E., Maximov, T.C., van Huissteden, J., and Berendse, F.: Permafrost collapse after shrub removal shifts tundra ecosystem to a methane source. Nat. Clim. Chang., 5, 67-70. https://doi.org/10.1038/nclimate2446, 2015.

Nelson, F. E., Shiklomanov, N. I., Hinkel, K. M, Christiansen, H H.: The Circumpolar active layer monitoring (CALM) Workshop and THE CALM II Program. Polar Geogr., 28(4): 253-266, https://doi.org/10.1080/789610205, 2004.

Nitu R, Roulet Y A, Wolff M, et al. WMO Solid Precipitation Intercomparison Experiment (SPICE) (2012-2015). Instruments and Observing Methods Rep. 131, World Meteorological Organization, 2018, 21445 pp., https://library.wmo.int/doc_num.php?explnum_id55686.

Obu, J., Westermann, S., Bartsch, A., Berdnikov, N., Christiansen, H. H., Dashtseren, A., Delaloye, R., Elberling, B., Etzelmüller, B., Kholodov, A., Khomutov, A., Kääb, A., Leibman, M. O., Lewkowicz, A. G., Panda, S. K., Romanovsky, V., Way, R. G., Westergaard-Nielsen, A., Wu, T., Yamkhin, J., and Zou, D.: Northern Hemisphere permafrost map based on TTOP modelling for 2000–2016 at 1 km^2 scale, Earth-Sci. Rev., 193, 299–316, https://doi.org/10.1016/j.earscirev.2019.04.023, 2019.

Park, H., Kim, Y., and Kimball, J. S.: Widespread permafrost vulnerability and soil active layer increases over the high northern latitudes inferred from satellite remote sensing and process model assessments, Remote Sens. Environ., 175, 349–358, https://doi.org/10.1016/j.rse.2015.12.046, 2016.

https://doi.org/10.5194/essd-2021-429
Preprint. Discussion started: 13 December 2021

Park, H., Launiainen, S., Konstantinov, P. Y., Iijima, Y., and Fedorov, A. N.: Modeling the effect of moss cover on soil temperature and carbon fluxes at a tundra site in northeastern Siberia. J. Geophys. Res.: Biogeosci., 123(9): 3028-3044, https://doi.org/ 10.1029/2018JG004491, 2018.

Romanovsky, V. E, Drozdov, D. S, Oberman, N. G., Malkova, G. V., Kholodov, A. L., Marchenko, S. S., Moskalenko, N. G., Sergeev, D. O., Ukraintseva, N. G., Abramov, A. A., Gilichinsky., D. A. and Vasiliev., A. A.: Thermal state of permafrost in Russia, Permafr. Periglac. Process., 21(2), 136-155, https://doi.org/10.1002/ppp.683, 2010.

Sun, G. J., and Zhao, S. L.: The study on vegetation of Mahan Mountain in Gansu (in Chinese). Acta Bot. Boreal.-Occid. Sin. 15(5), 115-120, 1995.

Van Everdingen, R. O.: Multi-Language Glossary of Permafrost and Related Ground-Ice Terms in Chinese, English, French, German, Icelandic, Italian, Norwegian, Polish, Romanian, Russian, Spanish, and Swedish. International Permafrost Association, Terminology Working Group, The Arctic Institute of North America, The University of Calgary, Alberta, Canada, https://globalcryospherewatch.org/reference/glossary_docs/Glossary_of_Permafrost_and_Ground-Ice_IPA_2005.pdf, 1998.

Walvoord, M. A., and Kurylyk, B. L.: Hydrologic impacts of thawing permafrost-a review. 15 (6), vzj2016.01.0010, https://doi.org/10.2136/vzj2016.01.0010, 2016.

Westermann, S., Langer, M., and Boike, J.: Spatial and temporal variations of summer surface temperatures of high-arctic tundra on Svalbard – Implications for MODIS LST based permafrost monitoring, Remote Sens. Environ., 115, 908–922, https://doi.org/10.1016/j.rse.2010.11.018, 2011.

Wu, T. and Xie, C.: Permafrost, active layer and meteorological data from a relict permafrost site at Mahan Mountain, Northeast of Qinghai-Tibet Plateau (2010–2020) Version 2.0. National Tibetan Plateau Data Center, https://doi.org/10.11888/Cryos.tpdc.271838, 2021.

Xie, C., Gough, W. A., Tam, A., Zhao, L., and Wu, T.: Characteristics and Persistence of Relict High-Altitude Permafrost on Mahan Mountain, Loess Plateau, China, Permafr. Periglac. Process., 24, 200-209, https://doi.org/10.1002/ppp.1776, 2013.

Zhang, T., Heginbottom, J. A., Barry, R. G., and Brown, J.: Further Statistics on the Distribution of Permafrost and Ground Ice in the Northern Hemispere, Polar Geogr., 24, 14–19,

https://doi.org/10.5194/essd-2021-429
Preprint. Discussion started: 13 December 2021

https://doi.org/10.1080/10889370009377692, 2000.

Zhang, Z., Wu, Q., and Xun, X., Li, Y.: Spatial distribution and changes of Xing'an permafrost in China over the past three decades. Quat. Int., 523:16-24, https://doi.org/10.1016/j.quaint.2019.06.007, 2019.

Zhao, L., and Sheng, Y. (Eds.): Permafrost Survey Manual, Science Press, Beijing, China, 2015.

Zhao, L., Wu, Q. B., Marchenko, S. S., and Sharkhuu, N.: Thermal state of permafrost and active layer in Central Asia during the International Polar Year. Permafr. Periglac. Process., 21(2), 198-207, https://doi.org/10.1002/ppp.688, 2010.

Zhao, L., Zou, D., Hu, G., Wu, T., Du, E., Liu, G., Xiao, Y., Li, R., Pang, Q., Qiao, Y., Wu, X., Sun, Z., Xing, Z., Sheng, Y., Zhao, Y., Shi, J., Xie, C., Wang, L., Wang, C., & Cheng, G.: A synthesis dataset of permafrost thermal state for the Qinghai-Xizang (Tibet) Plateau, China. Earth Syst. Sci. Data, 13, 4207–4218. https://10.5194/essd-13-4207-2021, 2021.

Zhao, Y., Chen, R., Han, C., Wang, L., Guo, S., Liu J.: Correcting precipitation measurements made with Geonor T-200B weighing gauges near the August-one ice cap in the Qilian Mountains, Northwest China, Journal of Hydrometeorology, 22(8): 1973-1985. https://doi.org/10.1175/JHM-D-20-0271.1, 2021.

Zou, D., Zhao, L., Sheng, Y., Chen, J., Hu, G., Wu, T., Wu, J., Xie, C., Wu, X., Pang, Q., Wang, W., Du, E., Li, W., Liu, G., Li, J., Qin, Y., Qiao, Y., Wang, Z., Shi, J., and Cheng, G.: A new map of permafrost distribution on the Tibetan Plateau, Cryosphere, 11, 2527-2542, https://doi.org/10.5194/tc-11-2527-2017, 2017.